

02,12

# On the Dirac mass of Hubbard fermions in strongly correlated higher-order topological superconductor

© S.V. Aksenov, A.D. Fedoseev, M.S. Shustin, A.O. Zlotnikov

Kirensky Institute of Physics, Federal Research Center KSC SB,  
Russian Academy of Sciences,  
Krasnoyarsk, Russia

E-mail: asv86@iph.krasn.ru

Received April 17, 2023

Revised April 17, 2023

Accepted May 11, 2023

Majorana corner modes have a number of advantages over the conventional Majorana states in terms of performing topologically protected quantum computations. However, the problem of the influence of Coulomb repulsion on higher-order phases, which inevitably arises when trying to implement such systems in practice, has been poorly studied. In this article, we analyze the features of a topological invariant describing the nontrivial phase with the corner modes for a two-dimensional two-orbital model of a hybrid structure in the regime of extremely strong electron correlations. For this purpose, approximate wave functions of the edge states with a linear dispersion law and the associated Dirac masses, which arise when superconducting pairing in the system is taken into account, are obtained.

**Keywords:** topological phases, Dirac fermions, Coulomb interaction, strong correlations, Majorana modes.

DOI: 10.61011/PSS.2023.07.56391.31H

## 1. Introduction

Two-dimensional higher-order topological superconductors and insulators differ from traditional ones in that the dimension of their gapless excitations is two less than the system dimension [1]. Majorana corner states occurring in superconducting systems are separated by an energy gap both from edge and bulk excitations. Taking into account strict localization in the 2D system corners, such objects may be more attractive in terms of topologically protected quantum computations than traditional Majorana states [2,3].

The Dirac mass sign change criterion is one of possible methods used to detect conditions for topological corner state occurrence in 2D systems. The criterion can be used provided that there is some interaction (e.g. superconducting pairing or hybridization) that breaks one of the traditional topological system symmetries and results in emergence of a mass term in the Dirac dispersion law for edge states. The sign of this mass shall be different on the adjacent sides of the 2D structure. This variable was used before as a topological index to describe occurrence of Majorana corner modes in various superconducting systems without many-body interaction [2,4–6].

It should be noted that lively discussion is being held now regarding which of the proposed invariants describes the higher-order topological phases to the fullest extent possible for interaction-free systems as well as for a situation when charge correlations play a significant role. In addition to the Dirac mass analysis, it is proposed to calculate topological indices on the bases of, for example, eigenvalues of inverse

Green's function [7], electric multipole moments [8,9], polarization and other quantum entanglement properties [10,11], Berry phase [12].

This article contains detailed analytical description of edge state wave functions of a 2D topological insulator and their Dirac mass that occurs when superconducting pairing is included and induces the nontrivial phase in a strong electron correlation regime at  $U \rightarrow \infty$  (where  $U$  is an on-site Coulomb repulsion intensity). The derived expressions are used to analyze the phase diagram of a higher-order topological superconductor (HOTSC) and define the applicability limits of a criterion based on the Dirac mass.

## 2. HOTSC Hamiltonian in strong electron correlation regime

The problem of higher-order topological superconductivity in strong correlation regime will be discussed using a model of 2D two-orbital topological insulator on a square lattice in the shape of a square that is expected to be on the surface of a high-temperature superconductor with  $s_{\pm}$ -type of order parameter symmetry [13], for example, iron-based [14]. Due to the proximity effect, superconducting pairing of the expanded  $s$ -type is induced in the 2D structure. It should be noted that the resulting relationship between the pairing amplitude and wave vector is a critical factor for appearance of different sign Dirac masses in edge states at adjacent boundaries. Significance of this circumstance for the implementation of correspondence between spectral properties of the system with periodic

boundary conditions along one of the directions and the system with open boundary conditions („edge-corner correspondence“) has been also stressed in [13]. However, the authors described these considerations outside the context of the Dirac mass.

As shown in [15], in the limit  $U \rightarrow \infty$ , when using the atomic representation, the Hamiltonian of this system reduces to the description of lower Hubbard subbands for each orbital and is written as

$$\begin{aligned} \mathcal{H} = & \sum_{f\sigma} \sum_{l=A,B} (-\mu + \eta_l \Delta \varepsilon) X_{fl}^{\sigma\sigma} \\ & + \sum_{f\sigma} \sum_{\delta=\pm x, \pm y} \eta_l t_\delta X_{fl}^{\sigma 0} X_{f+\delta,l}^{0\sigma} + \sum_{f\delta l\sigma} \alpha_{\sigma\delta} X_{fl}^{\sigma 0} X_{f+\delta,\bar{l}}^{0\bar{\sigma}} \\ & + \sum_{f\delta l} (\Delta_1 X_{fl}^{\uparrow 0} X_{f+\delta,l}^{0\downarrow} + \Delta_1^* X_{f+\delta,l}^{0\downarrow} X_{fl}^{\uparrow}), \end{aligned} \quad (1)$$

where  $l = A(B)$  is the orbital index for which  $\bar{l} = B(A)$ , respectively;  $\mu$  is the chemical potential,  $\Delta \varepsilon$  defines the one-site energy shift for different orbitals as a result of  $\eta_A = +1$ ,  $\eta_B = -1$ .

The Hubbard operators are defined in the standard form:  $X_{fl}^{nm} = |fl, n\rangle \langle fl, m|$ , where  $|fl, n\rangle$  are basic electron states on site  $f$  for orbital  $l$ . After projecting using operator  $P = \prod_f \sum_{l=A,B} (X_{fl}^{00} + X_{fl}^{\uparrow\uparrow} + X_{fl}^{\downarrow\downarrow})$  to a state subspace containing no state with two electrons on a site ( $n = 2$ ) in each orbital, a set of basic states is as follows:  $n = 0$  is a state without electrons,  $n = \sigma$  is a state with one electron with spin momentum projection  $\sigma$ . It should be noted that one-site states with two electrons from different orbitals are not allowed. Effect of the Hubbard operators on the state basis is defined as follows

$$X_{fl}^{nm} |f'l', p\rangle = \delta_{ff'} \delta_{ll'} \delta_{mp} |fl, n\rangle,$$

where  $\delta_{ij}$  are the Kronecker's symbols. Relation of the initial fermionic operators with the Hubbard operators before projection is written as  $c_{fl\sigma} = X_{fl}^{0\sigma} + \sigma X_{fl}^{\bar{\sigma}2}$ . It is easy to verify that, taking into account projection for Hamiltonian (1), transition between the operators is written as:  $X_{fl}^{0\sigma} = P c_{fl\sigma} P$ ,  $X_{fl}^{\sigma\sigma} = P c_{fl\sigma}^+ c_{fl\sigma} P$ . The Hubbard operator algebra is described in detail in [16,17].

In Hamiltonian (1), fermion hopping parameters satisfy relations  $t_{\pm x} = -t_{\pm y} = t$ . Whilst their opposite signs for different orbitals defined by factor  $\eta_l$  provides inverted bare electron bands. Spin-orbit coupling has properties  $\alpha_{\sigma, \pm x} = \mp \alpha \sigma$ ,  $\alpha_{\sigma, \pm y} = \pm i \alpha$ . The Cooper pairing amplitude on the nearest lattice sites is defined by  $\Delta_1$ . However, one-site Cooper pairings in limit  $U \rightarrow \infty$  are completely suppressed by the Hubbard repulsion.

### 3. Green's functions and the effective Hamiltonian

#### 3.1. Equations of motion for Green's functions

The equation of motion for operator  $X_{fl}^{0\sigma}(t)$  in the Heisenberg representation is written as:

$$\begin{aligned} i \frac{d}{dt} X_{fl}^{0\sigma}(t) = & (-\mu + \eta_l \Delta \varepsilon) X_{fl}^{0\sigma} \\ & + \sum_{\delta=\pm x, \pm y} t_\delta \eta_l [(X_{fl}^{00} + X_{fl}^{\sigma\sigma}) X_{f+\delta,l}^{0\sigma} + X_{fl}^{\bar{\sigma}\bar{\sigma}} X_{f+\delta,l}^{0\bar{\sigma}}] \\ & + \sum_{\delta} [\alpha_{\sigma\delta} (X_{fl}^{00} + X_{fl}^{\sigma\sigma}) X_{f+\delta,\bar{l}}^{0\bar{\sigma}} + \alpha_{\bar{\sigma}\delta} X_{fl}^{\bar{\sigma}\bar{\sigma}} X_{f+\delta,\bar{l}}^{0\bar{\sigma}}] \\ & + \sum_{\delta} \Delta_1 \sigma [(X_{fl}^{00} + X_{fl}^{\sigma\sigma}) X_{f+\delta,l}^{\bar{\sigma}0} - X_{fl}^{\bar{\sigma}\bar{\sigma}} X_{f+\delta,l}^{\sigma 0}]. \end{aligned} \quad (2)$$

Then we use the formalism of Green's two-time temperature functions defined as

$$\langle\langle A(t) | B(t') \rangle\rangle = -i \Theta(t - t') \langle \{A(t), B(t')\} \rangle, \quad (3)$$

where  $\Theta(t - t')$  is the Heaviside function,  $A(t)$  and  $B(t')$  are the arbitrary Hubbard operators in general. In order to calculate the fermionic excitation spectrum, the fermionic operators are chosen, so the brackets  $\{ \dots \}$  designate the anticommutator. We use the Hubbard-I approximation [18] with the simplest decoupling of equations of motion carried out for Green's functions with emergence of correlators

$$H_{fl\sigma} = \langle X_{fl}^{00} + X_{fl}^{\sigma\sigma} \rangle = 1 - \langle X_{fl}^{\bar{\sigma}\bar{\sigma}} \rangle. \quad (4)$$

The latter equality is derived from the Hubbard operator fullness condition. Correlators  $\langle X_{fl}^{\bar{\sigma}0} X_{fl}^{0\sigma} \rangle$  describing the fermion spin flip on the site are also not included in this approximation. In  $U \rightarrow \infty$  regime, the Hubbard-I approximation may be considered as a good first approximation against which correlation corrections can be considered (see, for example, [19–23]). Wherein some spectral [24] and superconducting [25,26] properties of strongly correlated systems are described adequately within the specified approximation.

It can be seen that the closed system of equations of motion in the used approximation is derived for a set of operators  $X_{fl}^{0\sigma}$ ,  $X_{fl}^{0\bar{\sigma}}$ ,  $X_{fl}^{\bar{\sigma}0}$ ,  $X_{fl}^{\sigma 0}$ . Then the system of equations for Green's functions in the designated state subspace in the quasi-momentum representation is written as

$$\begin{aligned} G^{-1}(k, \omega) \cdot \mathbf{V} = & \mathbf{C}; \quad (5) \\ G^{-1}(k, \omega) = & \begin{pmatrix} \omega - \xi_{kl} & \alpha_{kl\sigma} & -\sigma \Delta_{kl} & 0 \\ \alpha_{k\bar{l}\sigma}^* & \omega - \xi_{k\bar{l}} & 0 & \sigma \Delta_{k\bar{l}} \\ -\sigma \Delta_{kl}^* & 0 & \omega + \xi_{kl} & \alpha_{kl\sigma} \\ 0 & \sigma \Delta_{k\bar{l}}^* & \alpha_{k\bar{l}\sigma}^* & \omega + \xi_{k\bar{l}} \end{pmatrix}; \end{aligned}$$

$$\mathbf{V} = \begin{pmatrix} \langle\langle X_{kl}^{0\sigma} | B \rangle\rangle \\ \langle\langle X_{k\bar{l}}^{0\bar{\sigma}} | B \rangle\rangle \\ \langle\langle X_{kl}^{\sigma 0} | B \rangle\rangle \\ \langle\langle X_{k\bar{l}}^{\sigma 0} | B \rangle\rangle \end{pmatrix};$$

$$\mathbf{C} = \left( \langle\{X_{kl}^{0\sigma}, B\}\rangle, \langle\{X_{k\bar{l}}^{0\bar{\sigma}}, B\}\rangle, \langle\{X_{kl}^{\sigma 0}, B\}\rangle, \langle\{X_{k\bar{l}}^{\sigma 0}, B\}\rangle \right)^T.$$

Matrix  $G^{-1}$  involved herein is an equivalent of inverse matrix Green's function after analytical continuation derived in the Matsubara representation by the diagram technique in an approximation including only loopless diagrams (see, for example, [17,21,27]). The difference is that the correlators are calculated from the complete Hamiltonian, rather than from its diagonal part. The following notations are introduced

$$\begin{aligned} \xi_{kl} &= -\mu + \eta_l \Delta \varepsilon + 2\eta_l t_l (\cos k_x - \cos k_y), \\ \alpha_{kl\sigma} &= \alpha_l (\sin k_y + i\sigma \sin k_x), \\ \Delta_{kl} &= 2\Delta_l (\cos k_x + \cos k_y), \end{aligned} \quad (6)$$

where  $t_l = tH_l$ ,  $\alpha_l = 2\alpha H_l$  and  $\Delta_l = \Delta_1 H_l$  are renormalized hopping, spin-orbit coupling and Cooper pairing parameters between the nearest neighbors. In this case, the Hubbard renormalizations  $H_{f_l\sigma} \equiv H_l$  are homogeneous on the lattice and do not depend on the spin momentum projection, but at  $\Delta \varepsilon \neq 0$ , they are different for different orbitals.

### 3.2. The effective Hamiltonian

In order to calculate the excitation spectrum we proceed to a new „quasi-particle“ representation using an unitary matrix  $U$ :

$$G^{-1}\mathbf{V} \rightarrow \mathcal{G}^{-1}\tilde{\mathbf{V}} = UG^{-1}U^+U\mathbf{V} = UC,$$

where

$$\begin{aligned} \mathcal{G}^{-1} &= UG^{-1}U^+ \\ &= \text{diag}(\omega - E_{1k}, \omega - E_{2k}, \omega + E_{1k}, \omega + E_{2k}), \end{aligned}$$

which eigenvalues are  $E_{jk}$  ( $j = 1, 2$ ). The latter notation actually describes the effective Hamiltonian diagonalization problem

$$\tilde{H}(k) = \omega - G^{-1}(k). \quad (7)$$

To determine the Dirac mass, it is initially enough to perform diagonalization of this matrix for the topological insulator (without superconductivity,  $\Delta_1 = 0$ ). In this case the effective Hamiltonian matrix is represented as a direct sum of „Hamiltonians“ in the electron and hole subspaces

$$\tilde{H} = \tilde{H}_e \oplus \tilde{H}_h = \begin{pmatrix} \xi_{kl} & -\alpha_{kl\sigma} \\ -\alpha_{k\bar{l}\sigma}^* & \xi_{k\bar{l}} \end{pmatrix} \oplus \begin{pmatrix} -\xi_{kl} & -\alpha_{kl\sigma} \\ -\alpha_{k\bar{l}\sigma}^* & -\xi_{k\bar{l}} \end{pmatrix}. \quad (8)$$

Eigen vectors for matrices  $\tilde{H}_e$  and  $\tilde{H}_h$  will be designated as  $(u_{k\sigma}, w_{k\bar{\sigma}})^T$  and  $(v_{k\sigma}, z_{k\bar{\sigma}})^T$ , respectively.

In this approach, the Hubbard renormalizations  $H_l = 1 - \langle n_l \rangle / 2$  and correlators  $\langle n_l \rangle$  are also determined without considering the corrections for superconducting pairing amplitude ( $\Delta_1 = 0$ ). As a result, a self-consistent equation is derived from the correlator coupling with Green's function

$$\langle n_l \rangle \equiv \sum_{\sigma} \langle X_{f_l}^{\sigma 0} X_{f_l}^{0\sigma} \rangle = H_l I_0 + \eta_l H_l I_1,$$

$$I_0 = \sum_k (f_{1k} + f_{2k}),$$

$$I_1 = \sum_k \frac{1}{\lambda_k} [\Delta \varepsilon + (H_A + H_B)t_k/2](f_{2k} - f_{1k}), \quad (9)$$

where  $f_{1,2k}$  are the Fermi-Dirac functions corresponding to the spectrum branches of topological insulator  $\varepsilon_{1,2k}$  with the periodic boundary conditions

$$\varepsilon_{1,2k} = -\mu + \frac{H_A - H_B}{2} t_k \mp \lambda_k,$$

$$\lambda_k = \sqrt{(\Delta \varepsilon + (H_A + H_B)t_k/2)^2 + \alpha_{kA\sigma}\alpha_{kB\bar{\sigma}}}. \quad (10)$$

Further, the excitation spectra and Dirac masses are calculated in the zero temperature limit and the temperature corrections in (9) are ignored.

### 3.3. Continual description

Consider the system in the vicinity of symmetric points  $(k_{x0}, k_{y0}) = (0, \pi)$ ,  $(k_{x0}, k_{y0}) = (\pi, 0)$  at which inversion of the topological insulator bands can occur [13]. Then,

$$\cos k_x \rightarrow c_x - \frac{1}{2} c_x (k_x - k_{x0})^2;$$

$$\sin k_x \rightarrow c_x (k_x - k_{x0}); \quad c_x = \cos k_{x0}, \quad (11)$$

$$\cos k_y \rightarrow c_y - \frac{1}{2} c_y (k_y - k_{y0})^2;$$

$$\sin k_y \rightarrow c_y (k_y - k_{y0}); \quad c_y = \cos k_{y0}, \quad (12)$$

Then, to proceed to the continuum description, the following replacements are made

$$k_x - k_{x0} \rightarrow -i\partial_x, \quad k_y - k_{y0} \rightarrow -i\partial_y,$$

and electronlike and holelike wave functions of the effective Hamiltonian with quasi-momenta  $p$  and  $q$ , respectively, will be written as:

$$\begin{aligned} \begin{pmatrix} u_{k\sigma} \\ w_{k\bar{\sigma}} \end{pmatrix} &\sim \begin{pmatrix} u_{\sigma} \\ w_{\bar{\sigma}} \end{pmatrix} e^{i(p_x x + p_y y)}; \\ \begin{pmatrix} u_{k\sigma} \\ z_{k\bar{\sigma}} \end{pmatrix} &\sim \begin{pmatrix} u_{\sigma} \\ z_{\bar{\sigma}} \end{pmatrix} e^{i(q_x x + q_y y)}, \end{aligned} \quad (13)$$

where vectors  $(u_{\sigma}, w_{\bar{\sigma}})^T$  and  $(v_{\sigma}, z_{\bar{\sigma}})^T$  have a meaning of envelope electronlike and holelike wave functions. Proceeding to the continuum description, the eigenproblem

for the electron subspace will be written as (further  $m_l = -\mu + \eta_l \Delta \varepsilon + 2t_l \eta_l (c_x - c_y)$ ):

$$(E - \mathcal{H}_e) \mathbf{U}_e = \begin{pmatrix} E - m_l + \eta_l t_l (c_x p_x^2 - c_y p_y^2) & \alpha_l (c_y p_y + i \sigma c_x p_x) \\ \alpha_l (c_y p_y - i \sigma c_x p_x) & E - m_l - \eta_l t_l (c_x p_x^2 - c_y p_y^2) \end{pmatrix} \times \begin{pmatrix} u_{l\sigma} \\ w_{l\bar{\sigma}} \end{pmatrix} = \begin{pmatrix} 0 \\ 0 \end{pmatrix}. \quad (14)$$

Wherein the problem for the hole subspace  $(E - \mathcal{H}_h) \mathbf{U}_h = \mathbf{0}$  can be derived from the above problem by replacement  $m_l \rightarrow -m_l$ ,  $t_l \rightarrow -t_l$ . Therefore, the obtained results will be further also generalized to this case.

It should be noted that system of equations (14) shall be expanded to calculate the excitation spectrum and edge mode wave functions in the spatially limited lattice, because the Hubbard renormalizations become dependent on the coordinate. However, to determine the Dirac masses whose ratio plays a role of topological invariant in higher-order topological systems and to plot a topological phase diagram, it will be sufficient to consider an idealized boundary for which correlators  $\langle n_l \rangle$  are defined from equation (9) derived for the periodic boundary conditions, and Hamiltonian parameters (1) are unchanged near the boundaries. In other words, a real system with boundaries shall be described taking into account the appropriate corrections that, however, do not result in change of fundamental conclusions regarding the existence and implementation area of topologically protected states. Such approach has been used, for example, in [15,28].

In this regard, to calculate the topological invariant, we will use the system of equations for homogeneous correlators case (14) for which the type of solution depends on the considered lattice boundary. To find conditions for realization of topological corner states on the square-form lattice, it is sufficient to use simple cases:

– in the case of the boundary along the  $Ox$  axis,

$$p_x \rightarrow p, \quad p_y \rightarrow i\lambda : \Im(p) = 0, \quad \Re(\lambda) > 0,$$

– in the case of the boundary along the  $Oy$  axis,

$$p_x \rightarrow iv, \quad p_y \rightarrow q : \Im(q) = 0, \quad \Re(v) > 0.$$

#### 4. Dirac mass calculation

The case when the system boundary is along the  $Ox$  axis will be discussed in detail. Then, the Schrödinger equation will be written as

$$(E - \mathcal{H}_e) \mathbf{U}_e = \begin{pmatrix} E - m_l + \eta_l t_l (c_x p^2 + c_y \lambda^2) & i \alpha_l (c_y \lambda + \sigma c_x p) \\ i \alpha_l (c_y \lambda - \sigma c_x p) & E - m_l - \eta_l t_l (c_x p^2 + c_y \lambda^2) \end{pmatrix} \times \begin{pmatrix} u_{l\sigma} \\ w_{l\bar{\sigma}} \end{pmatrix} = \begin{pmatrix} 0 \\ 0 \end{pmatrix}. \quad (15)$$

The condition for the solution existence is

$$\det(E - \mathcal{H}_e) = -t_{AtB} \lambda^4 + (b_1 E + b_0) \lambda^2 + (E^2 + c_1 E + c_0) = 0, \quad (16)$$

where

$$\begin{aligned} b_1 &= c_y (t_A - t_B); \\ b_0 &= -2c_x c_y t_{AtB} p^2 + \alpha_A \alpha_B - c_y (t_A m_B - t_B m_A); \\ c_1 &= c_x (t_A - t_B) p^2 - m_A - m_B; \\ c_0 &= -t_{AtB} p^4 - (c_x (t_A m_B - t_B m_A) + \alpha_A \alpha_B) p^2 + m_A m_B. \end{aligned} \quad (17)$$

Then we have two solutions for  $r = \lambda^2$ :

$$r_{1,2} = \frac{b_1 E + b_0}{2t_{AtB}} \pm \frac{\sqrt{(b_1 E + b_0)^2 + 4t_{AtB} (E^2 + c_1 E + c_0)}}{2t_{AtB}}. \quad (18)$$

In the used approach for edge states whose wave functions decay with distance from the boundary, solutions shall satisfy condition  $\Re(\lambda) > 0$ . Then in the parameter area of interest, roots  $r_{1,2}$  are complex conjugate. In this case

$$\begin{aligned} \lambda_1 \neq \lambda_2 &\implies \Psi(x, y) \\ &= C_1 \begin{pmatrix} u_{1l\sigma} \\ w_{1l\bar{\sigma}} \end{pmatrix} e^{ipx - \lambda_1 y} + C_2 \begin{pmatrix} u_{2l\sigma} \\ w_{2l\bar{\sigma}} \end{pmatrix} e^{ipx - \lambda_2 y}. \end{aligned} \quad (19)$$

Using the edge condition  $\Psi(x, y = 0) = 0$ , equations for  $C_{1,2}$  are derived:

$$\begin{pmatrix} u_{1l\sigma} & u_{2l\sigma} \\ w_{1l\bar{\sigma}} & w_{2l\bar{\sigma}} \end{pmatrix} \begin{pmatrix} C_1 \\ C_2 \end{pmatrix} = \begin{pmatrix} 0 \\ 0 \end{pmatrix};$$

$$\begin{aligned} u_{1,2;l\sigma} &= -i \alpha_l (c_y \lambda_{1,2} + \sigma c_x p); \\ w_{1,2;l\bar{\sigma}} &= E - m_l + \eta_l t_l (c_x p^2 + c_y \lambda_{1,2}^2). \end{aligned} \quad (20)$$

Solvability condition of this system reduces to equation

$$\eta_l \sigma c_x t_l p (\lambda_1 + \lambda_2) = -\eta_l c_y t_l \lambda_1 \lambda_2 + E - (m_l - \eta_l c_x t_l p^2). \quad (21)$$

For  $\lambda_{1,2}$ , the following relations are satisfied

$$\lambda_1^2 \lambda_2^2 = -\frac{E^2 + c_1 E + c_0}{t_{AtB}}; \quad \lambda_1^2 + \lambda_2^2 = \frac{b_1 E + b_0}{t_{AtB}}. \quad (22)$$

These combinations may be obtained by twice squaring equation (21). As a result, we obtain the equation of the 4-th degree by  $\omega$  which, as can be easily seen, has a linear-in- $p$  solution (with  $t > 0$ ,  $\alpha > 0$ ):

$$\begin{aligned} E &= \sigma c_x s (p - p_0); \quad s = 4 \frac{H_A H_B}{H_A + H_B} \alpha, \\ p_0 &= -\sigma c_x \frac{-\mu (H_A + H_B) - \Delta \varepsilon (H_A - H_B)}{4 H_A H_B \alpha}. \end{aligned} \quad (23)$$

The case without the Coulomb interaction is restored from (23), if we put  $H_A = H_B = 1$ . In this case, it can be seen that  $p_0 = 0$  at  $\mu = 0$  and the Dirac cone is centered

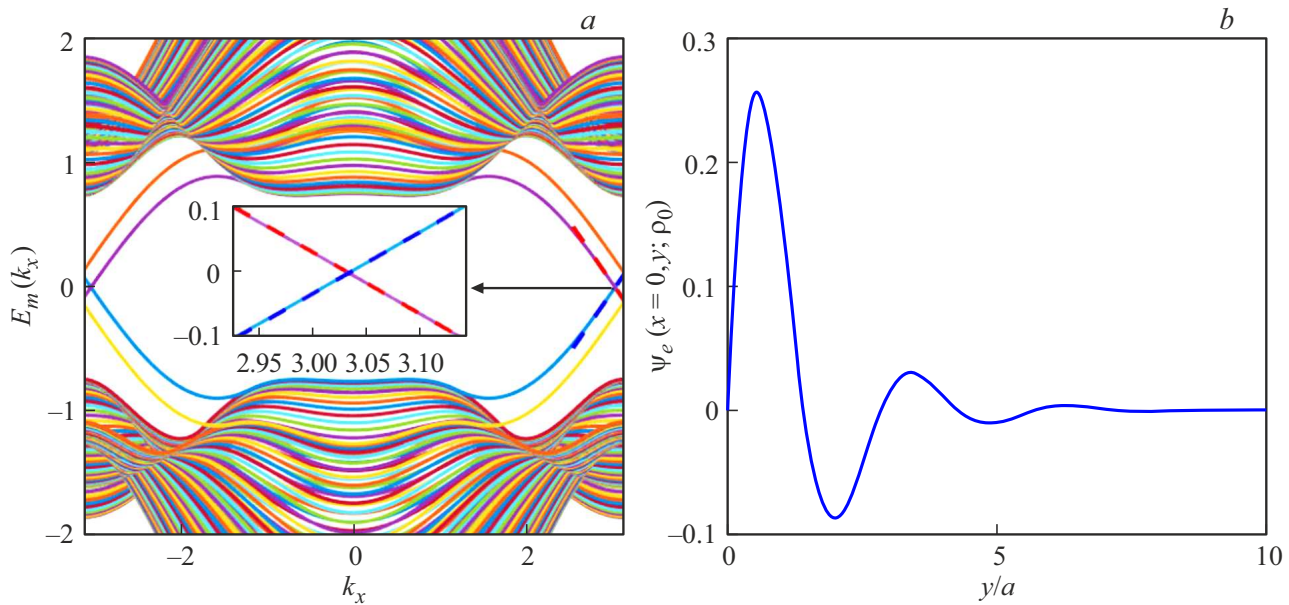


**Figure 1.** *a)* System excitation spectrum: solid lines — numerical diagonalization of the effective Hamiltonian (7) with the periodic boundary conditions along the  $Ox$  axis with 1000 sites and open boundary conditions along the  $Oy$  axis with 100 sites; various solid lines correspond to various values of  $m$ ; dashed lines — calculations using equation (23). Detail — scaled-up Dirac spectrum of edge states. *b)* Electronlike wave function behavior for the quasi-momentum corresponding to the vertex of the Dirac spectrum cone;  $a$  — lattice constant. System parameters in units  $t$ :  $\mu = -0.25$ ,  $\alpha = 3/4$ ,  $\Delta\varepsilon = 1$ ,  $k_{x0} = \pi$ ,  $k_{y0} = 0$ ,  $\sigma = +1$ .

precisely in the expansion point (in this case  $k_{x0} = \pi$ ). Existence of the Hubbard renormalizations in the strong correlation regime results in the moving of the Dirac point in particular, at  $\mu = 0$  (displacement from point  $k_{x0}$  is defined by  $p_0$ ). Comparison of the analytical expression for the linear part of the excitation spectrum (dashed lines) and numerical calculation of the system spectrum (solid lines) with the boundary along the  $Ox$  axis are shown in Figure 1. Comparison of the analytical and numerical calculations is shown on the left side of Figure 1. The numerical calculations were carried out by diagonalization of the effective Hamiltonian (7) with the periodic boundary conditions along direction  $Ox$  and open boundary conditions along direction  $Oy$ . This allowed to introduce quasi-momentum  $k_x$ . While the Hubbard renormalizations  $H_I$  in equation (4) were calculated self-consistently with the excitation spectrum  $E_{k_x}$  on the assumption of the periodic boundary conditions along both spatial directions. The analytical finding of the Dirac spectrum was carried out using equation (23). Similar equations for the hole components may be obtained by replacement  $E \rightarrow E$ , which are also shown in Figure 1. It can be easily seen that the Dirac spectrum occurs symmetrically and for negative quasi-momenta.

Using self-consistent equations (9), the Hubbard renormalization combinations included in (23) may be written as

$$\frac{H_A H_B}{H_A + H_B} = \frac{1}{2 + I_0}, \quad \frac{H_A H_B}{H_A - H_B} = -\frac{1}{I_1}. \quad (24)$$

In the most interesting case, when the chemical potential lies in the gap between the spectrum branches  $\varepsilon_{1,2k}$  and edge states occur,  $I_0 = 1$  in the zero temperature limit. Then, when strong correlations are considered, the Dirac cone slope coefficient is 1.5 times lower than that in the case when no interaction exists, for which  $s = 2\alpha$ .

Using the solution of the system (20), the general form of edge states wave functions can be written as

$$\Psi_{Ox}^{(e)}(x, y; p) = \frac{1}{\sqrt{\mathcal{N}_x \mathcal{N}_y}} F_y e^{ipx},$$

where normalization factors are  $\mathcal{N}_x = \int_0^{L_x} dx$ ,  $\mathcal{N}_y = \int_0^\infty (F_y^+ F_y) dy$ ,  $L_x = N_x a$  is the lattice size along the  $Ox$  axis, and

$$F_y = \begin{pmatrix} u_{1\sigma} u_{2\sigma} \\ w_{1\bar{\sigma}} u_{2\sigma} \end{pmatrix} e^{-\lambda_1 y} - \begin{pmatrix} u_{1\sigma} u_{2\sigma} \\ u_{1\sigma} w_{2\bar{\sigma}} \end{pmatrix} e^{-\lambda_2 y}. \quad (25)$$

However, as mentioned above, the case when  $\lambda_1 = \lambda_2^* = \lambda$  is of interest. In this case, the wave function expression may be reduced to a simple form. For such simplification, assume that from system of equations (20) follows  $\omega_{1\bar{\sigma}} u_{2\sigma} = u_{1\sigma} \omega_{2\bar{\sigma}}$ . Then, from (20) we get  $u_{1\sigma} = -u_{2\sigma}^*$  and  $w_{1\bar{\sigma}} = w_{2\bar{\sigma}}^*$ . Finally, we deduce  $w_{2\bar{\sigma}} = i u_{2\sigma}$ . Then, the following expressions for the edge state wave functions may be derived easily

$$\Psi_{Ox}^{(e)}(x, y; p) = \sqrt{\frac{2\lambda'}{\mathcal{N}_x}} \begin{pmatrix} |\lambda| \\ |\lambda''| \end{pmatrix} \begin{pmatrix} -i \\ 1 \end{pmatrix} e^{ipx - \lambda'y} \sin(\lambda''y). \quad (26)$$

$$\Psi_{Ox}^{(h)}(x, y; p) = \sqrt{\frac{2\lambda'}{\mathcal{N}_x}} \left( \frac{|\lambda|}{|\lambda''|} \right) \begin{pmatrix} -i \\ -1 \end{pmatrix} e^{ipx - \lambda'y} \sin(\lambda''y). \quad (27)$$

In the latter expressions  $\lambda' = \Re(\lambda)$ ,  $\lambda'' = \Im(\lambda)$ . Taking this into account, we obtain the final expression for the Dirac mass in case of the boundary along the  $Ox$  axis (it is sufficient to consider  $p = p_0$ ):

$$\begin{aligned} M_{Dx} &= (\Psi_{Ox}^{(e)}, \hat{\Delta}\Psi_{Ox}^{(h)}) \\ &= \frac{1}{2} \Delta_1 \sigma (H_A + H_B) [2(c_x + c_y) - c_x p_0^2 - c_y |\lambda|^2]; \\ \hat{\Delta} &= \sigma \Delta_1 (2c_x + 2c_y + c_x \partial_x^2 + c_y \partial_y^2) \begin{pmatrix} H_I & 0 \\ 0 & -H_I \end{pmatrix}; \\ |\lambda|^2 &= \sqrt{\frac{t_A t_B p_0^4 + (c_x (t_A m_B - t_B m_A) + \alpha_A \alpha_B) p_0^2 - m_A m_B}{t_A t_B}}. \end{aligned} \quad (28)$$

Operator  $\hat{\Delta}$  was obtained from off-diagonal matrix blocks (5) when proceeding to the continual description.

Acting in the similar way, the edge state wave functions can be easily derived for the periodic boundary conditions along the  $Oy$  axis and for the open boundary conditions along the  $Ox$  axis:

$$\Psi_{Oy}^{(e)}(x, y; q) = i \sqrt{\frac{2\nu'}{\mathcal{N}_y}} \left( \frac{|\nu|}{|\nu''|} \right) \begin{pmatrix} -1 \\ 1 \end{pmatrix} e^{iqy - \nu'x} \sin(\nu''x), \quad (29)$$

$$\Psi_{Oy}^{(h)}(x, y; q) = i \sqrt{\frac{2\nu'}{\mathcal{N}_y}} \left( \frac{|\nu|}{|\nu''|} \right) \begin{pmatrix} -1 \\ -1 \end{pmatrix} e^{iqy - \nu'x} \sin(\nu''x). \quad (30)$$

In the latter expression  $\nu' = \Re(\nu)$ ,  $\nu'' = \Im(\nu)$ ,  $\mathcal{N}_y = \int_0^{L_y} dy$ ,  $L_y = N_y a$  is the lattice size along the  $Oy$  axis. Therefore, the matrix element of the interaction operator caused by the proximity-induced superconducting pairing at the boundary along the  $Oy$  axis is written as:

$$\begin{aligned} M_{Dy} &= (\Psi_{Oy}^{(e)}, \hat{\Delta}\Psi_{Oy}^{(h)}) \\ &= \frac{1}{2} \Delta_1 \sigma (H_A + H_B) [2(c_x + c_y) - c_x |\nu|^2 - c_y q_0^2]; \\ |\nu|^2 &= \sqrt{\frac{t_A t_B q_0^4 - (c_y (t_A m_B - t_B m_A) - \alpha_A \alpha_B) q_0^2 - m_A m_B}{t_A t_B}}, \\ q_0^2 &= p_0^2. \end{aligned} \quad (31)$$

## 5. Topological invariant for the corner modes

Sign change of the Dirac mass at the adjacent idealized boundaries of the 2D higher-order topological superconductor is known to indicate the generation of topologically protected corner Majorana modes. Therefore, ratio of the

Dirac masses obtained by the described approach on the boundaries along the  $Ox$  and  $Oy$  axes may serve as a topological invariant equivalent for such states:

$$\frac{M_{Dx}}{M_{Dy}} = \frac{2(c_x + c_y) - c_x p_0^2 - c_y |\lambda|^2}{2(c_x + c_y) - c_x |\nu|^2 - c_y p_0^2}. \quad (32)$$

For the given points  $(k_{x0}, k_{y0})$   $c_x = -c_y$ . Then  $|\nu|^2 = |\lambda|^2$  and the Dirac mass relation is equal to  $-1$  throughout the region where the solution with linear spectrum exists (23). This region is defined from the condition that the bulk energy spectrum of the topological insulator (without superconducting pairings) with the periodic boundary conditions has a gap, i.e. the chemical potential is between the lower Hubbard subbands (see (10)). Therefore, the calculations use the Hubbard renormalizations defined exactly by equations (9) without considering the boundary effects. The boundaries of this phase are shown in Figure 2 on the diagram in variables  $\mu - \Delta\varepsilon$  with solid light lines for parameters  $\alpha = 3/4$ ,  $\Delta_1 = 0.5$ , and the phase itself is designated as  $MCM_1$ .

As shown above, the superconducting pairings in this phase induce a mass in the Dirac spectrum of the topological insulator, and, since the Dirac masses for the adjacent boundaries have different signs, may result in appearance of the Majorana corner modes in the 2D system with open boundary conditions. When the chemical potential intersects the Hubbard subbands, the bulk spectrum becomes gapless and, thus, the type of solution at zero energy in the restricted system changes and includes the contributions from the bulk states and from the boundaries. Therefore, in this parameter region, the developed approach to the Dirac mass calculation becomes inappropriate.

Generally, when proceeding to the spatially limited 2D lattice, the excitation energy of the Majorana corner modes depends only on overlapping of localized mode wave functions at different corners. Thus, with the increase in the lattice sizes (the number of sites  $N_{x,y}$  along the boundary), the excitation energy of the Majorana corner modes becomes exponentially low  $\sim \exp(-N_{x,y})$ , and the energy of the next (in order of magnitude) excitation is defined by the Dirac mass  $\sim \Delta_1$  and corresponds to the state localized along the lattice boundaries.

However, the corner modes with zero energy may exist inside a wider region whose boundaries are shown in Figure 2 by dark solid lines. These lines define the boundaries between the nodal phases designated as  $N$ , where the bulk excitation spectrum is gapless, even when superconducting pairings are considered, and the regions with the gap in the bulk spectrum induced by the superconductivity. It should be noted that these boundaries are defined from the analysis of the quasi-particle spectrum of the system with the periodic boundary conditions calculated using (5) and taking into account the Cooper pairings. For this system, the Hubbard renormalizations are spatially homogeneous on the lattice. Thus, in the regions enclosed between the dark and light solid lines and designated as  $MCM_2$ ,

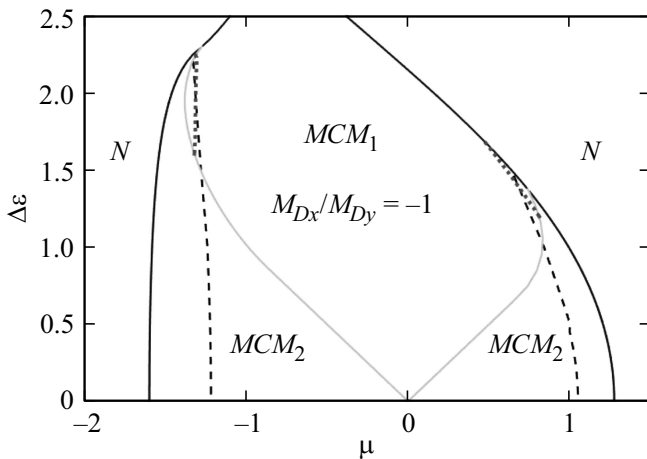


**Figure 2.** The topological phase diagram of HOTSC with phase  $MCM_1$  in which the Dirac mass ratio equal to  $-1$  allows implementation of the Majorana corner modes. In phase  $MCM_2$ , the Dirac solution is absent, however, the Majorana corner modes can appear in it as well (the explanation is given in the text herein). In nodal phases  $N$ , HOTSC bulk spectrum is gapless and no topological states occur. Dashed lines show the gap closure conditions in the HOTSC edge spectrum for the discussed approximate approach, however, no topological transitions occur on these lines. The dotted lines in phase  $MCM_1$  are approximate solutions obtained from Dirac mass vanishing. Parameters  $\alpha = 3/4$ ,  $\Delta_1 = 0.5$ .

other corner mode formation mechanism is implemented that is different from that described above. In regions  $MCM_2$ , the bulk spectrum of the topological insulator is gapless, therefore (26)–(29) type solutions are absent when the idealized boundaries are addressed. Incorporation of superconductivity induces the gap both in the bulk and edge spectra, instead of only resulting in the generation of the Dirac mass in the linear spectra along the boundaries like in phase  $MCM_1$ . Whilst for the 2D system with open boundary conditions in parametric phases  $MCM_2$ , zero corner modes may also occur (see [15]). Figure 2 shows that when superconductivity is incorporated, transition between phases  $MCM_1$  and  $MCM_2$  may be implemented without any gap closure in the spectrum (to the left of the dashed line in the region of the negative chemical potential values and to the right of the dashed line with positive  $\mu$ ). Consequently, the corner modes in phases  $MCM_2$  can be also of Majorana type.

In [15], regions where topologically trivial phases are implemented in the considered model were found and designated as 0. Figure 2 does not show these phases, because they border on phases  $N$  with lower and higher chemical potential values than the range of  $\mu$  addressed herein. Whilst these regions are trivial without edge states, because they correspond either to fully empty or fully filled Hubbard bands in the topological insulator model. Therefore the approach using the Dirac masses is also inapplicable in these phases like in regions  $N$  and  $MCM_2$ .

It should be noted that the Dirac masses may vanish. The analytical expressions derived within the described approximate approach for the parameters at which  $M_{D_x} = M_{D_y} = 0$  are written as (in accordance with the Dirac point position in Figure 1,  $c_x = -1$  is considered herein):

$$\Delta\epsilon_{c1,2} = -\mu \frac{H_A + H_B}{H_A - H_B} - 2 \frac{H_A H_B}{H_A - H_B} \frac{H_A + H_B}{H_A - H_B} \frac{\alpha^2}{t} + 2 \frac{H_A H_B}{H_A - H_B} \frac{\alpha}{t} \sqrt{\left(\frac{H_A + H_B}{H_A - H_B}\right)^2 \alpha^2 + 8t^2 + 4 \frac{\mu t}{H_A - H_B}}. \quad (33)$$

The obtained solutions are shown by dotted lines in Figure 2. As noted above, the Hubbard factors included in expression (33) do not depend on the site number in the lattice and shall satisfy self-consistent equations (9) with the selected parameters. New combinations of Hubbard renormalizations may be also represented through integrals  $I_0, I_1$  calculated in (9):

$$\frac{H_A + H_B}{H_A - H_B} = -\frac{2 + I_0}{I_1}, \quad \frac{1}{H_A - H_B} = -\frac{(2 + I_0)^2 - I_1^2}{4I_1}. \quad (34)$$

Then using (24), expression (33) may be rewritten in terms of  $I_0$  and  $I_1$  that, however, depend on  $H_A, H_B$ .

Zero Dirac masses indicate that the gap in the edge spectrum is closed when superconducting pairings are taken into account. These conditions shall be considered only in phase  $MCM_1$  with  $M_{D_x}/M_{D_y} = -1$ , because the Dirac solution is absent in other regions. Figure 2 shows that the dotted lines with zero Dirac masses in phase with  $M_{D_x}/M_{D_y} = -1$  are formed only near the phase boundaries. However, as shown above, the gapless excitations induced on these lines do not change relation  $M_{D_x}/M_{D_y} = -1$  and do not result in the topological transition.

The dashed lines show the conditions for gapless excitation occurrence in the edge spectrum of the higher-order topological superconductor which were obtained within the numerical solution when constant correlator values on the lattice were also addressed (9). It can be seen that in phase  $M_{D_x}/M_{D_y} = -1$ , the analytical approximate solution is near the numerical one. The differences are caused by the fact that displacement  $p_0$  from points  $(k_{x0}, k_{y0})$  near the phase boundaries increases up to  $\approx 0.5$ , as a result the expansion (11) becomes inaccurate. The most well-developed approach is applicable far from the boundaries inside phase  $MCM_1$  (see Figure 1).

It should be noted that the boundary effects, e.g. dependence of the Hubbard renormalizations on the distance from the lattice boundaries may change the dashed line position. However, this will not affect the topological phase diagram description as long as the dashed line intersects the region of phase  $MCM_1$ . The fact that implementation of gapless excitations in the edge spectrum in this phase of the higher-order topological superconductor does not result in any change of the topological invariant — the Dirac mass ratio and, therefore, topological phase transition, means that the

topological states in regions  $MCM_2$  have to be equivalent to the states in  $MCM_1$ . It should be noted that in [13,15] such transition was induced by means of variation of  $\Delta_0$  of the on-site superconducting pairings which were completely suppressed when the Coulomb repulsion is high. As a result, the Majorana corner modes shall be induced both on the left and on the right of the dashed lines in regions  $MCM_2$ .

## 6. Conclusions

To calculate the topological invariant — the Dirac mass ratio on the adjacent boundaries of the higher-order topological superconductor when ensemble of the Hubbard fermion is formed in the extremely strong Coulomb correlation regime (interaction parameter  $U \rightarrow \infty$ ), approximate analytical expressions were obtained for the edge state wave functions near the boundaries of the 2D lattice and the corresponding Dirac energy spectrum with neglecting any heterogeneities near the boundary. This allowed to describe in detail the topologically non-trivial phase which admits the appearance of the Majorana zero modes in the restricted 2D system.

Compared with the results for the model without interactions, the approximate Dirac spectrum obtained for the Dirac mass calculation taking into account the correlations has a smaller angle and displaced Dirac point. Like in the case without interactions, superconducting pairings that occur, for example, due to the proximity effect in the topological insulator–superconductor structure result in opening of the energy gap in the edge excitation spectrum (non-zero Dirac mass). It is shown that, throughout the parametric region where the described solutions are implemented, the Dirac masses on the adjacent boundaries of the square lattice have different signs resulting to the implementation of a higher-order topological superconducting phase where the Majorana modes localized in the lattice corners shall be formed.

Possibility of corner mode appearance is also demonstrated in the restricted parameter regions with gapless excitations in the bulk energy spectrum of the topological insulator obtained when the periodic boundary conditions along both square lattice directions are addressed. In these regions, the Dirac solution for edge conditions is absent and the Dirac mass calculation approach offered herein is not applicable. However, in this case Cooper pairings may induce the gap both in the bulk and edge spectrum. It is shown that these phases may be coupled with the phase with non-trivial Dirac mass ratio on different boundaries by means of parameter variation without gap closure in both types of spectra. Thus, the corner modes occurring in the considered regions are also topologically protected.

It is proved that gap closure in the edge spectrum in the higher-order topological superconductivity phase does not result in any topological phase transition. Other parameter regions correspond to the nodal phases where the bulk

spectrum remains gapless even when superconductivity is present or to topologically trivial phases described above.

## Funding

The study was supported by the Russian Science Foundation (project No. 22-22-20076), and Krasnoyarsk Regional Fund of Science.

## Conflict of interest

The authors declare that they have no conflict of interest.

## References

- [1] A.O. Zlotnikov, M.S. Shustin, A.D. Fedoseev. *J. Supercond. Nov. Magn.* **34**, 3053 (2021).
- [2] S.-B. Zhang, W.B. Rui, A. Calzona, S.-J. Choi, A.P. Schnyder, B. Trauzettel. *Phys. Rev. Res.* **2**, 043025 (2020).
- [3] S.-B. Zhang, A. Calzona, B. Trauzettel. *Phys. Rev. B* **102**, 100503(R) (2020).
- [4] J. Langbehn, Y. Peng, L. Trifunovic, F. von Oppen, P.W. Brouwer. *Phys. Rev. Lett.* **119**, 246401 (2017).
- [5] E. Khalaf. *Phys. Rev. B* **97**, 205136 (2018).
- [6] A.D. Fedoseev. *Phys. Rev. B* **105**, 155423 (2022).
- [7] H. Li, H.-Y. Kee, Y.B. Kim. *Phys. Rev. B* **106**, 155116 (2022).
- [8] W.A. Benalcazar, B.A. Bernevig, T.L. Hughes. *Phys. Rev. B* **96**, 245115 (2017).
- [9] W.A. Wheeler, L.K. Wagner, T.L. Hughes. *Phys. Rev. B* **100**, 245135 (2019).
- [10] T. Fukui, Y. Hatsugai. *Phys. Rev. B* **98**, 035147 (2018).
- [11] Y. You, J. Bibo, F. Pollmann. *Phys. Rev. Res.* **2**, 033192 (2020).
- [12] H. Araki, T. Mizoguchi, Y. Hatsugai. *Phys. Rev. Res.* **2**, 012009 (2020).
- [13] Q. Wang, C.-C. Liu, Y.-M. Lu, F. Zhang. *Phys. Rev. Lett.* **121**, 186801 (2018).
- [14] P.J. Hirschfeld, M.M. Korshunov, I.I. Mazin. *Rev. Mod. Phys.* **74**, 124508 (2011).
- [15] S.V. Aksenov, A.D. Fedoseev, M.S. Shustin, A.O. Zlotnikov. *Phys. Rev. B* **107**, 125401 (2023).
- [16] Yu.A. Izyumov. *Physics–Uspekhi* **40**, 445 (1997).
- [17] V.V. Valkov, S.G. Ovchinnikov. *Kvazichastitsy v silno korrelirovannykh sistemakh*. SO RAN, Novosibirsk (2001). (in Russian). *Hubbard Operators in the Theory of Strongly Correlated Electrons*, Imperial College Press, London (2004).
- [18] J. Hubbard. *Proc. Roy. Soc. A* **276**, 238 (1963).
- [19] P.O. Zaitsev. *JETP* **43**, 574 (1976).
- [20] E.V. Kuzmin, S.G. Ovchinnikov. *Theoretical and Mathematical Physics* **31**, 523 (1977).
- [21] V.V. Valkov, D.M. Dzebisashvili. *JETP* **107**, 679 (2008).
- [22] V.V. Valkov, D.M. Dzebisashvili. *Phys. Solid State* **51**, 877 (2009).
- [23] V.V. Valkov, M.M. Korovushkin. *JETP* **112**, 108 (2011).
- [24] C. Grober, R. Eder, W. Hanke. *Phys. Rev. B* **62**, 4336 (2000).
- [25] R.O. Zaitsev, V.A. Ivanov. *FTT*, **29**, 2554 (1987). (in Russian).
- [26] A.V. Rozhkov, A.L. Rakhmanov. *J. Phys. Condens. Matter* **23**, 065601 (2011).
- [27] V.V. Valkov, A.O. Zlotnikov. *JETP Letters* **104**, 483 (2016).
- [28] V.V. Valkov. *JETP Letters* **111**, 647 (2020).

*Translated by Ego Translating*